Measurements of dielectric loss factors due to a Martian dust analog

Kevin K. Williams[1] and Ronald Greeley
Department of Geological Sciences, Arizona State University, Tempe, Arizona, USA

Received 10 July 2002; revised 2 August 2004; accepted 18 August 2004; published 15 October 2004.

[1] Radar signals can penetrate loose sediments such as dust, sand, and alluvium to reveal buried geologic structures obscured in visible and infrared images. In anticipation of data from instruments such as the MARSIS and SHARAD radar sounders and potential future imaging SAR and rover-mounted GPR instruments, measurements have been made to characterize electrical loss factors of a Martian dust analog and an iron-rich soil. This paper presents results from dielectric measurements of Carbondale Red Clay (CRC) and the palagonitic Mars JSC-1 soil simulant from 0.2 to 1.3 GHz and from transmission measurements of radar penetration of CRC up to 12 GHz. Attenuations predicted from dielectric measurements are compared to values measured in the experiment and are discussed relative to the frequencies at which imaging radars operate. Over the frequencies considered, loss tangent, tan δ, decreases with increasing frequency, but attenuation increases due to the influence of wavelength. Attenuation in CRC ranges from 8 to 22 dB/m over P and L bands and jumps to 36 and 67 dB/m at C and X bands, respectively. Mars JSC-1 has lower attenuation of 5 dB/m at P band and $\sim$12 dB/m at L band. Compared to attenuation measurements of sand, both CRC and Mars JSC-1 cause significantly greater attenuation, likely due to their compositions containing iron-bearing minerals. Because Martian fine sediments also contain ferric mineral components, constraining higher losses of analogs for Martian dust and fine sediments is important for predicting the performance of radar instruments operating in orbit or on the surface of Mars. *INDEX TERMS:* 5464 Planetology: Solid Surface Planets: Remote sensing; 6225 Planetology: Solar System Objects: Mars; 6297 Planetology: Solar System Objects: Instruments and techniques; 5470 Planetology: Solid Surface Planets: Surface materials and properties; *KEYWORDS:* attenuation, Mars, radar

Citation: Williams, K. K., and R. Greeley (2004), Measurements of dielectric loss factors due to a Martian dust analog, *J. Geophys. Res.*, *109*, E10006, doi:10.1029/2002JE001957.

1. Introduction

[2] Visible and thermal infrared imaging data of Mars have thus far provided information about only the top $\sim$0.5 cm of the Martian surface. Widespread aeolian deposits reflect the current and past wind regimes on Mars [e.g., *McCauley et al.*, 1972; *Cutts and Smith*, 1973; *Greeley et al.*, 1992; *Malin and Edgett*, 2001], but they also obscure structures that hold information about the geologic history of Mars. The Mars Advanced Radar for Subsurface and Ionosphere Sounding (MARSIS) and Shallow Radar (SHARAD) orbital radar sounders and potential orbital synthetic aperture radar (SAR) and rover-mounted ground penetrating radar (GPR) instruments operate at frequencies that penetrate sand and dust and could provide information about obscured structures. Specifically, SAR data could provide a global map of the surface of Mars at microwave frequencies [e.g., *Thompson et al.*, 2000; *Campbell et al.*, 2001; *Paillou et al.*, 2001] that would be complementary to previous and current Mars imaging data sets.

[3] SAR has been a useful remote sensing tool for geologic investigations on Earth and Venus [e.g., *Schaber et al.*, 1986; *Greeley et al.*, 1995; *Campbell et al.*, 1997]. Orbital SAR images (Figure 1) revealed ancient river channels in Egypt that are now covered by windblown sand [e.g., *McCauley et al.*, 1982]. L band (λ = 25 cm) radar from the SIR-A instrument penetrated several meters of sand to the bedrock surface but was absorbed by thicker sand filling river channels. This resulted in dark dendritic patterns that reveal past fluvial activity (Figure 1). Because much of the Martian surface is obscured by windblown materials (Figure 2), radar missions have the potential to provide further information about the geologic and climatic history in those areas of Mars. However, it is important to understand radar signal losses due to aeolian materials expected on Mars in order to predict the amount of penetration expected at various radar frequencies.

[4] Results are presented here for dielectric measurements of Carbondale Red Clay (CRC) and the palagonitic Mars JSC-1 soil simulant from 0.2 to 1.3 GHz. These results are used to predict signal attenuation for P band (λ = 68 cm) and L band frequencies. Results are also presented for a laboratory experiment in which the transmission of microwaves through CRC was measured at C and X bands. The measured transmission was related to attenuation at those bands. The

[1] Now at Center for Earth and Planetary Studies, National Air and Space Museum, Smithsonian Institution, Washington, D. C., USA.

0148-0227/04/2002JE001957$09.00

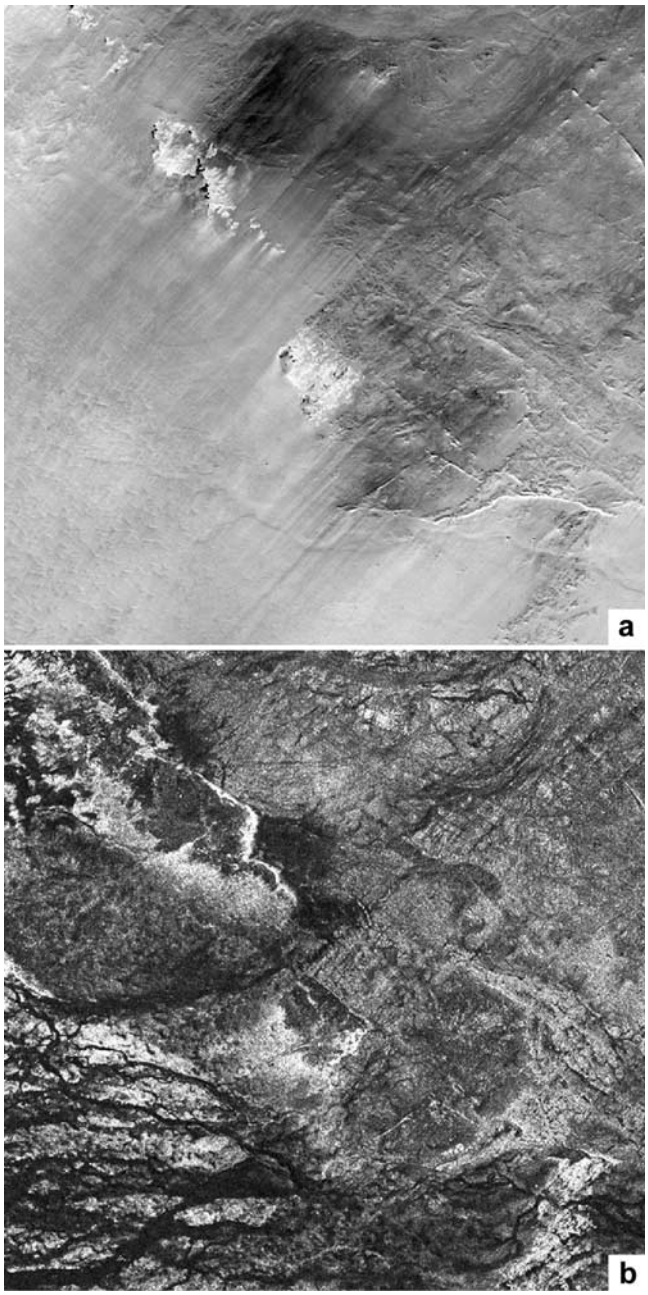

Figure 1. Comparison of visible and radar images of a sand-covered region. (a) Gray scale optical Landsat TM image of the Safsaf Oasis region, Egypt. Image is 24 km across. (b) Gray scale SIR-C/X-SAR composite image of the same area revealing obscured river channels and other features (L-hh, C-hh, and X-vv composite image) (NASA/JPL).

measured losses and calculated attenuations are discussed relative to frequency and the potential for radar at P band through X band to penetrate loose surface materials such as dust and sand to reveal obscured geologic features on Mars.

2. Background

2.1. Subsurface Imaging

[5] Field research in areas where orbital SAR resulted in subsurface imaging began with studies in the Sahara where

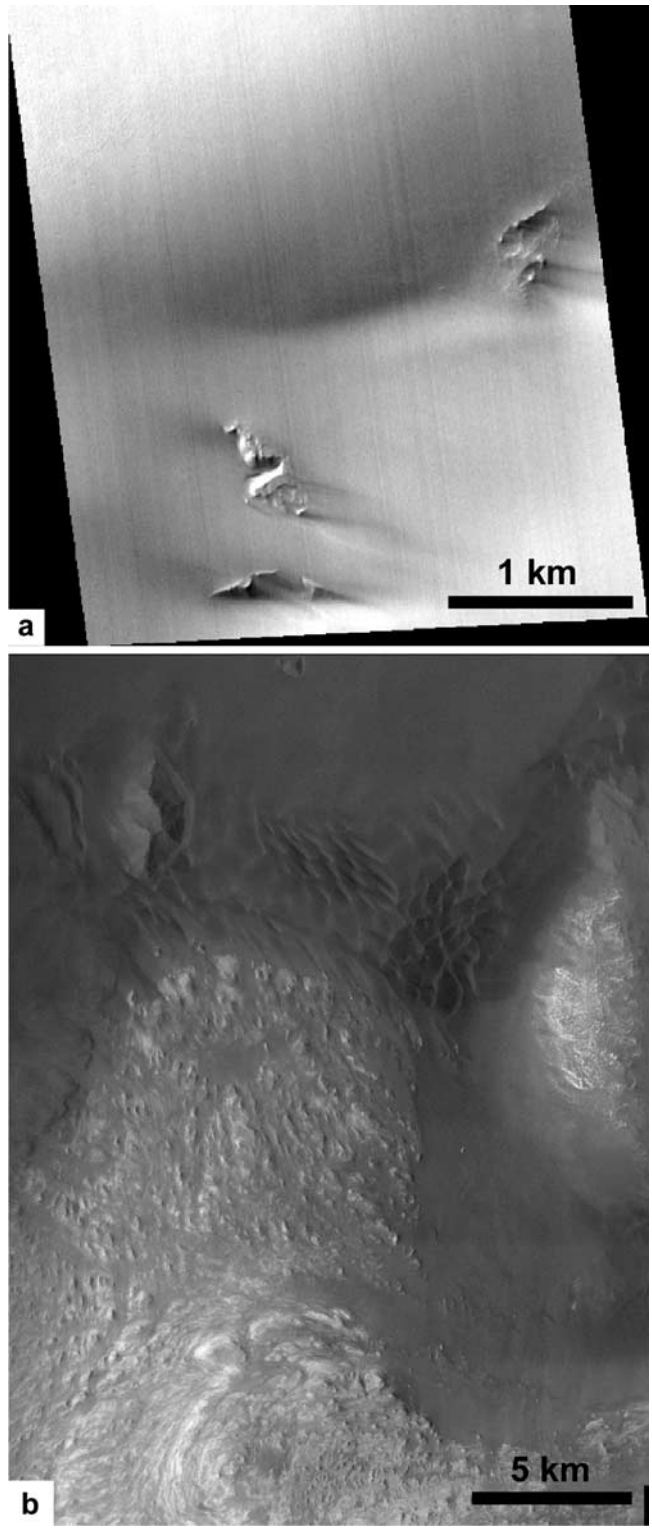

Figure 2. Images of Ganges Chasma showing areas where bedrock is obscured by sand. (a) Mars Global Surveyor MOC image (M00-00030) of a thick sand sheet in Ganges Chasma. Most of the underlying structure is obscured. Image is ~3 km across (NASA/JPL/MSSS). (b) Mars Odyssey THEMIS image of sand obscuring bedrock in low-lying areas. Image is ~20 km across (NASA/JPL/ASU).

SIR-A L band radar penetrated windblown sands [*McCauley et al.*, 1982]. These images added greatly to understanding the climatic history of the area by revealing ancient river channels. Subsequent studies have extended to China, Saudi Arabia, and the U.S. Southwest where radar subsurface imaging also occurred [*Blom et al.*, 1984; *Elachi et al.*, 1984; *Berlin et al.*, 1986; *Farr et al.*, 1986; *Guo et al.*, 1986; *Schaber et al.*, 1986; *Davis et al.*, 1993].

[6] More recently, studies using SIR-C/X-SAR and AIRSAR data have compared the abilities of different frequency and polarization combinations to discriminate buried geologic features [*Dabbagh et al.*, 1997; *Schaber et al.*, 1997; *Lancaster et al.*, 2000]. Studying multifrequency data led *Schaber and Breed* [1999] to note the need for further laboratory and field studies of radar penetration of loose sediments at various frequencies. *Williams and Greeley* [2001] quantified the decrease in radar signal strength as a function of frequency and soil moisture as radar signals were transmitted through sand (particles >60 microns in diameter). While confirming that low-frequency signals experience very little attenuation as they pass through dry sand, the experiment also showed that intermediate and higher frequencies experience sufficiently low signal attenuation that they might also be considered for radar missions to Mars.

2.2. Mars Radar

[7] Radar instruments operating at Mars will complement and supplement compositional and geomorphic information about the Martian surface being returned from visible and infrared instruments [e.g., *Christensen et al.*, 2001, 2003; *Malin and Edgett*, 2001]. Radar sounders such as MARSIS on Mars Express [*Safaeinili et al.*, 2001] and SHARAD on the 2005 Mars Reconnaissance Orbiter [*Seu et al.*, 2003] operate at frequencies expected to penetrate hundreds of meters to several kilometers to detect subsurface structure and to search for water. In addition to penetrating deeply, surface echoes from MARSIS and SHARAD could also return information about surficial geology obscured by aeolian deposits. Imaging radars discussed for Mars [e.g., *Thompson et al.*, 2000; *Campbell et al.*, 2001; *Paillou et al.*, 2001] would operate at frequencies that will not penetrate consolidated rock and could be used to study surfaces now covered by dust or sand. A rover-mounted GPR would potentially penetrate rock to depths of 10s of meters [*Grant et al.*, 2003] and would easily penetrate unconsolidated material while also providing structural information about aeolian deposits. In anticipation of Mars radar sounders, imaging radars, and surface GPRs, it is advantageous to measure the dielectric properties of Mars analog materials to predict signal losses from Martian surface materials.

2.3. Martian Dust

[8] In situ information about the composition of Martian dust (particles a few microns in diameter) comes from measurements performed at the Viking, Pathfinder, and Mars Exploration Rover landing sites. Chemical analyses performed by the XRFS instrument on the Viking landers and by the APXS on the Sojourner rover at Sagan Memorial Station suggested that Martian dust is composed of silicate particles with a ferric mineral component (possibly maghemite and/or magnetite) [*Clark et al.*, 1982; *Banin et al.*, 1992; *Hviid et al.*, 1997; *Rieder et al.*, 1997; *Bell et al.*, 1998]. Early results from the Spirit and Opportunity rovers suggest that dust particles at those landing sites are very similar to dust measured at the Pathfinder site [*Bell et al.*, 2004; *Gellert et al.*, 2004; *Hviid et al.*, 2004; *Morris et al.*, 2004]. Because radar signal penetration is influenced by dielectric properties of the penetrated materials [*Olhoeft and Capron*, 1993, 1994], measurements of those properties for Martian analog dust and other materials can help anticipate radar performance on Mars.

[9] Several previous laboratory studies have measured signal loss in analog Martian materials of various types. Some of the more recent studies used measurements of dielectric properties and simulations of radar propagation to discuss potential radar performance on Mars [e.g., *Pettinelli et al.*, 2001; *Heggy et al.*, 2003; *Leuschen et al.*, 2003a, 2003b]. On the basis of lander measurements, measurements of SNC meteorites, analogy with lunar samples, and Earth-based radar reflectivity data [*Downs et al.*, 1973; *Olhoeft and Strangway*, 1974, 1975; *Olhoeft*, 1989; *Christensen and Moore*, 1992; *Heggy et al.*, 2001; *Pettinelli et al.*, 2001; *Leuschen et al.*, 2003b], the dielectric constant for Martian materials was estimated at 2.5 to 9. However, a relatively high loss was measured in the imaginary part of the permittivity of some samples [*Leuschen*, 1999; *Heggy et al.*, 2001; *Pettinelli et al.*, 2001; *Leuschen et al.*, 2003b], suggesting that expected signal loss might be greater than that predicted from real permittivity measurements alone. This highlights the need to consider both aspects of permittivity to estimate signal loss.

[10] Because of the absence of in situ dielectric measurements of Martian surface material, previous selection of soil and dust analogs has been necessarily based on grain size, shape, and composition [e.g., *White et al.*, 1997; *Allen et al.*, 1998]. Studies trying to match composition have determined that montmorillonite, nontronite, palagonite, Carbondale Red Clay, and other materials may all be suitable simulants of Martian dust [*Hunt et al.*, 1973; *Toulmin et al.*, 1977; *White et al.*, 1997], and a palagonitic material collected from Mauna Kea, Hawaii (Mars JSC-1 soil simulant) is often used as an analog for Martian sediment [*Allen et al.*, 1998]. While considering possibilities for a dust simulant for use in wind tunnel studies, *White et al.* [1997] determined that Carbondale Red Clay (CRC) was the most appropriate analog on the basis of its physical characteristics and composition. Following the analysis of *White et al.* [1997], CRC was chosen as the dust analog for this study. CRC is a red pottery clay with main element components of ~56% SiO_2, 19% Al_2O_3, and 12% Fe_2O_3, and an average grain size of 2 μm. The CRC mainly consists of kaolinite contaminated with quartz, hematite, and chlorite [*White et al.*, 1997].

3. Dielectric Properties

3.1. Measurements

[11] Most previous studies of radar penetration of geologic materials have considered sand [e.g., *Schaber et al.*, 1986; *Mätzler*, 1998; *Williams and Greeley*, 2001], coarse alluvium (gravel, cobbles, etc.) [*Farr et al.*, 1986], or soil mixtures of sand, silt, and clay [e.g., *Ulaby et al.*, 1986]. *Hoekstra and Delaney* [1974] measured the dielectric prop-

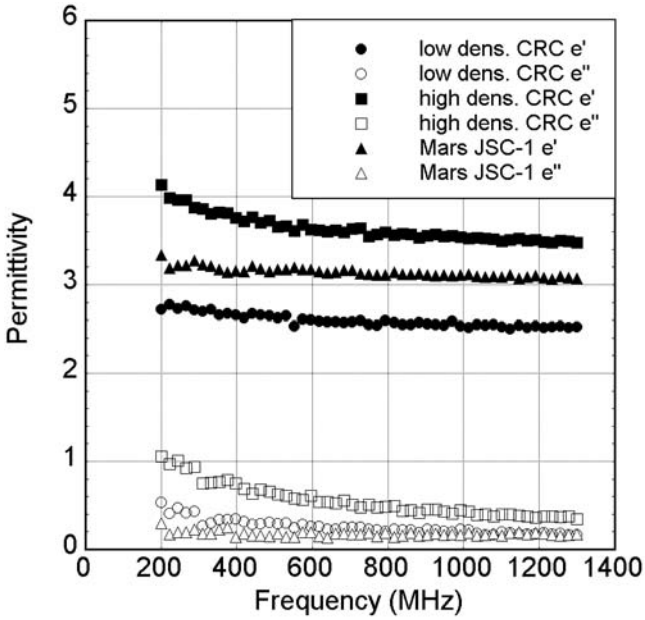

Figure 3. Dielectric properties as a function of frequency for CRC and Mars JSC-1. Solid symbols are real permittivity (ε'), and open symbols are the imaginary portion of permittivity (ε''). Values are given for loose and compacted CRC.

erties of various soil materials (including clay) at different moisture levels, but the clay they used was not iron-rich as Martian dust is expected to be. Therefore the present state of understanding about the electrical properties of Martian analog materials can be expanded by further inclusion of dielectric measurements of appropriate analogs for Martian dust and fine sediment.

[12] In order to understand better the expected radar signal loss due to Mars dust, this study measured the dielectric properties of Carbondale Red Clay, and the dielectric properties of Mars JSC-1 were also measured for comparison to a coarser-grained Mars soil simulant. The complex permittivity was measured from 0.2 to 1.3 GHz at the Particulate Media Research Lab at Georgia Institute of Technology. Because the density of material can affect penetration of radar waves [e.g., *Christensen and Moore*, 1992; *Campbell*, 2002], measurements were made for material loosely added to the sample container and for material that had been tamped to a greater density. The dielectric properties for CRC and Mars JSC-1 are shown in Figure 3, and Table 1 lists the real (ε') and imaginary (ε'') parts of the complex permittivity at P band and L band radar frequencies. Differences in dielectric values between loose and tamped samples were noticeable for CRC (Figure 3) but were small for Mars JSC-1 and are incorporated into the measurement errors for Mars JSC-1 in Table 1.

3.2. Analysis

[13] To discuss how Martian dust might affect radar signals, measurements of dielectric values were used to calculate loss tangents ($\tan\delta = \varepsilon''/\varepsilon'$) and signal attenuations at P and L bands for the CRC and Mars JSC-1 materials (Table 1). Signal attenuation in decibels per meter is calculated by

$$\text{attenuation} = 8.686 \bullet \left(\frac{2\pi}{\lambda_o}\right) \bullet \left[\frac{\varepsilon'}{2} \bullet \left(\sqrt{1+\tan^2\delta} - 1\right)\right]^{0.5}, \quad (1)$$

where free space wavelength, λ_o, is in meters [*Von Hippel*, 1954].

[14] At P band, the attenuation in CRC ranges from 8–15 dB/m, depending on the density, and the attenuation in Mars JSC-1 is 5.3 dB/m. At L band, Mars JSC-1 and the lower-density CRC have approximately the same attenuation at ~12 dB/m, but the attenuation almost doubles to 22.4 dB/m for CRC at higher density.

[15] Both ε' and ε'' decrease with increasing frequency from 0.2 to 1.3 GHz (Figure 3), however the decrease in ε'' dominates the effect on tan δ, causing tan δ to also decrease over that frequency range. Although loss tangent decreases with increasing frequency, the attenuation increases from P band to L band (Table 1) because of the effect of decreasing λ_o in equation (1).

[16] Because sand deposits are also widespread on Mars, it is worthwhile to compare the values in Table 1 to dielectric properties of clean sand [*Williams and Greeley*, 2001, 2004] and sand and alluvium from Egypt [*Schaber et al.*, 1986] (Table 2). Although these materials might not be ideal analogs for Mars, they were extremely dry, as would be expected for Martian surface materials. The loss tangents and attenuations are lower for the dry sand than for CRC and Mars JSC-1. The higher losses associated with CRC and Mars JSC-1 are likely due to the iron content of

Table 1. Dielectric Properties and Predicted Attenuations of CRC and Mars JSC-1

Band	Frequency, GHz	Wavelength, cm	ε'	ε''	tan δ	Attenuation, dB/m
			Lower-Density CRC			
P	0.5	60	2.63 ± 0.14	0.284 ± 0.014	0.108	7.9
L	1.24	24	2.51 ± 0.13	0.175 ± 0.009	0.070	12.6
			Higher-Density CRC			
P	0.5	60	3.72 ± 0.10	0.628 ± 0.006	0.169	14.8
L	1.24	24	3.47 ± 0.09	0.367 ± 0.004	0.106	22.4
			Mars JSC-1 Soil Simulant			
P	0.5	60	3.18 ± 0.10	0.207 ± 0.017	0.065	5.3
L	1.24	24	3.09 ± 0.09	0.180 ± 0.008	0.058	11.6

Table 2. Dielectric Properties and Predicted Attenuations of Sand and Alluvium

Band	Frequency, GHz	Wavelength, cm	ε'	ε''	tan δ	Attenuation, dB/m
			Dry Sand[a]			
P	0.5	60	2.11 ± 0.12	0.022 ± 0.015	0.0103	0.68
L	1.24	24	2.11 ± 0.14	0.008 ± 0.005	0.0038	0.63
			Dry Sand[b]			
L	1.5	20	3.62 ± 0.08	—	0.007–0.010	1.5–2.2
			Coarse Sand/Small Pebble Alluvium[b]			
L	1.5	20	3.35 ± 0.30	—	0.010–0.045	2.0–10.0

[a]Measurements of "#60 Silver Sand" used in experiments of *Williams and Greeley* [2001, 2004].
[b]Samples from Safsaf Oasis, Egypt. Measurements reported by *Schaber et al.* [1986].

those materials, whereas the sand has negligible amounts of iron. These differences illustrate the importance of considering appropriate analog compositions for Mars materials. This point is reinforced by the differences in properties between the #60 Silver Sand from California and the aeolian sand from Egypt (Table 2).

4. Microwave Transmission

4.1. Experimental Setup

[17] To address the issue of radar signal loss by dust at higher frequencies and through a different method, an experiment was performed to measure the change in transmitted microwave energy as a function of dust thickness using CRC as the Martian dust analog. The experiment was conducted in the Electromagnetic Anechoic Chamber at Arizona State University, where interference from the chamber itself is minimized [*Birtcher*, 1992]. The facility was designed for radar cross section measurements, but the radar emitters and receivers were arranged for vertical transmission measurements through a sample container (Figure 4). The base of the sample container was made of plywood, and the sides were made of Plexiglas to allow observation of the sample level during addition of CRC. The radar emitter was supported above the sample container between supports on dense foam blocks and the receiver was positioned beneath the container. Radar-absorbing material was placed below the receiver to minimize reflections from the floor.

[18] During the experiment, 801 measurements were acquired over each of four, slightly overlapping frequency ranges from 0.5 to 12 GHz using three radar emitter/receiver sets. Following measurements of the transmitted signal through the empty sample container, measurements were repeated for dust thicknesses of 10, 20, 30, and 40 cm. CRC was added loosely to the sample container to simulate settling of dust from the atmosphere but it could have compacted slightly under its own weight. The CRC was dry with a volumetric moisture content less than 0.5 percent. On the basis of other measurements of dielectric properties for materials with increasing water content [e.g., *Hoekstra and Delaney*, 1974; *Wang and Schmugge*, 1980], the dielectric properties of a material with small amounts of moisture do not vary greatly over the frequency range considered here, even for water contents up to 5%. Therefore it is expected that losses measured here are dominated by the effects of compositional properties, especially the effects of metal-bearing minerals.

4.2. Data Processing

[19] To consider the change in transmitted signal due to signal attenuation by the dust, raw data were normalized to the behavior of the empty sample container (Figure 5a). Although there is minor scatter in the data above 6 GHz, data between 2 and 6 GHz display variations that are more pronounced for thicker dust. These variations may be the result of interference from the sample container and of the

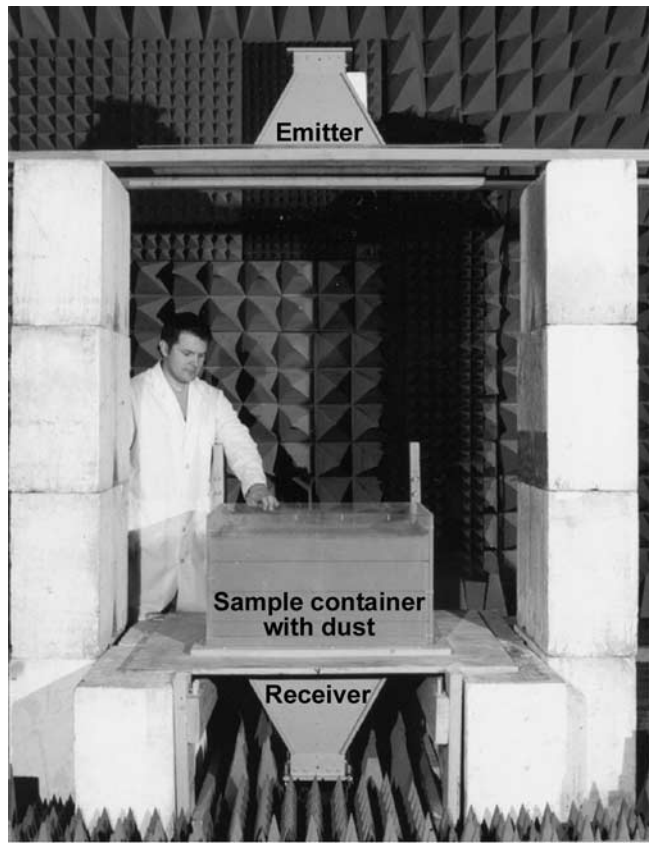

Figure 4. Experimental setup for transmission measurements through CRC. Radar emitter is suspended above the sample container. This image shows the dust at a level of 40 cm.

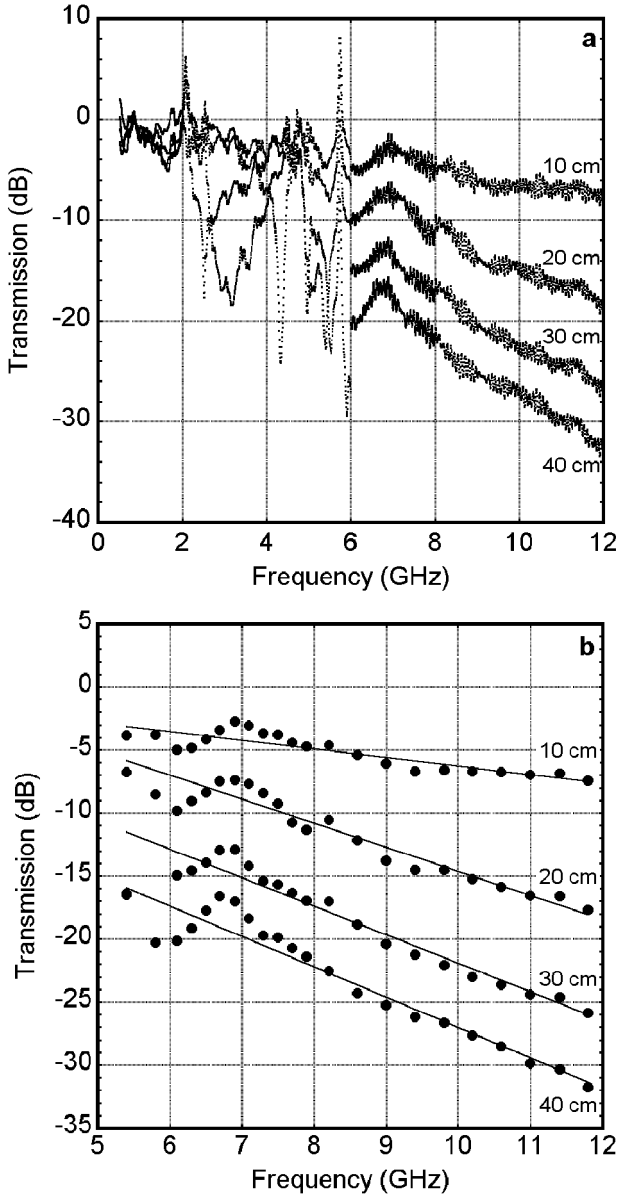

Figure 5. Transmission as a function of frequency for normalized data. (a) Normalized, unaveraged data at the four dust levels. (b) Normalized, averaged data at the four dust levels over the frequency range used for analysis.

dust being thin relative to the radar wavelength. Recognizing that the experiment was not ideal for lower-frequency measurements, only data from ~5.5 to 12 GHz are considered here. Those data were averaged to 21 data points to remove minor scatter, such as that caused by the plywood base.

[20] The averaged data were fit with linear curves to produce equations describing the change in signal as a function of frequency at each dust level (Figure 5b), and those equations were used to calculate the detected signal at C and X bands for each dust level. These data were plotted as a function of dust thickness and fit with linear curves (Figure 6), which were forced to intersect the origin because no attenuation would be expected if no dust were present. The lines were also extrapolated to 1 m of dust to estimate signal attenuations (dB/m) at C and X bands (Table 3).

4.3. Analysis

[21] As expected, signal attenuations measured at C and X bands are greater than for P and L bands calculated from dielectric properties. The variation with frequency is shown in Figure 7 where P and L band attenuations from Table 1 are shown as open symbols and values at C and X bands (Table 3) are shown as solid symbols. It is possible to fit curves through the data to describe the attenuation as a function of frequency with an equation, but variations due to density differences between the two experiments cannot be recovered. Instead, the trend of increasing attenuation with frequency can be qualitatively described as generally linear over the range from P band to X band. This is the range of imaging radars on Earth, and it is expected that a Mars SAR would operate at a frequency toward the lower end of that range (P or L band) to enable deeper penetration. Therefore a Mars SAR instrument could encounter a ~5–20 dB/m of signal attenuation in areas covered by fine-grained, metal-bearing material.

[22] In an effort to comment on tan δ values at C and X bands, it is necessary to make assumptions about ε'. If ε' does not vary greatly with frequency for dry materials [*Mätzler*, 1998], data in Figure 3 can be used to define three possible values of ε' (2.5, 3.0, and 3.5). Table 3 gives tan δ values predicted by inserting these possible permittivities and C and X band attenuation values into equation (1). Derived values of ε'' are also given. Compared to values of tan δ in Table 1, values shown in Table 3 are a further decrease with increasing frequency over the range studied here.

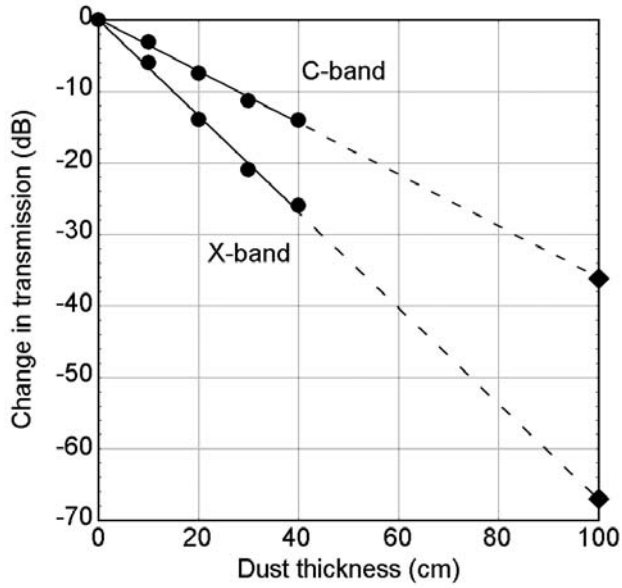

Figure 6. Transmission as a function of dust thickness for C band and X band. Values extracted from Figure 5b are shown as solid circles and have been extrapolated to 1 m (diamonds) to estimate signal attenuation in dB/m.

Table 3. Experiment-Derived Attenuations and Estimated Dielectric Properties of CRC

Band	Frequency, GHz	Attenuation, dB/m	Possible Permittivity	Band	tan δ	ε″
C	5.3	35.7 ± 2.7	if ε′ = 2.5	C	0.047	0.118
X	9.6	67.4 ± 0.9		X	0.048	0.120
			if ε′ = 3.0	C	0.043	0.129
				X	0.044	0.132
			if ε′ = 3.5	C	0.040	0.140
				X	0.041	0.144

Table 4. Skin Depths for Three Materials at Imaging Radar Bands[a]

Band	CRC	Mars JSC-1	Dry Sand[b]	Dry Sand[c]
P	0.59–1.09	1.65	—	12.8
L	0.39–0.69	0.75	3.4–5.7	13.8
C	0.24	—	—	1.3–2.6
X	0.13	—	—	0.7–1.7

[a]Skin depths are in meters.
[b]From *Schaber et al.* [1986].
[c]Based on attenuations presented by *Williams and Greeley* [2004].

[23] CRC used in the experiments (and even sand from the hyper-arid Sahara) contains more moisture than would be expected in Martian sediments. Therefore loss tangents and attenuations reported here are maximum values for comparable Martian materials because the surface of Mars should be sufficiently cold and dry to prevent loss due to dielectric relaxation of the water molecule. The laboratory used in this study could not operate below room temperature, but other studies will address material properties at temperatures below 0°C (M. Mellon, personal communication, 2004).

5. Discussion

[24] Because the penetrating ability of a radar instrument depends on many factors including the signal to noise sensitivity of the receiving antenna, the most direct way to present the potential penetration of different materials is by discussing the "skin depth" ($1/\alpha = 8.686/\text{attenuation}$), or the depth at which the signal power decreases to 1/e ($\sim$37%) of its incident strength. Table 4 lists skin depths calculated from the dielectric properties of CRC and Mars JSC-1. For comparison, skin depths are also listed for dry sand [*Schaber et al.*, 1986; *Williams and Greeley*, 2004]. Skin depths for CRC and Mars JSC-1 are significantly less than those for both sands listed, likely due to the relatively high metal contents in both CRC and Mars JSC-1. The greater skin depth at L band than at P band for sand from *Williams and Greeley* [2004] is the result of attenuations at those frequency bands being generally the same in that study. Results in Table 4 suggest that, at P band, radar would penetrate CRC-like dust to a depth less than 10% of the depth penetrated in clean sand similar to the #60 Silver Sand used by *Williams and Greeley* [2004]. As noted above, the considerable difference between penetration of sand and metal-bearing dust reinforces the need to consider compositions of Martian analog materials and how they compare to compositions derived from in situ measurements at Mars.

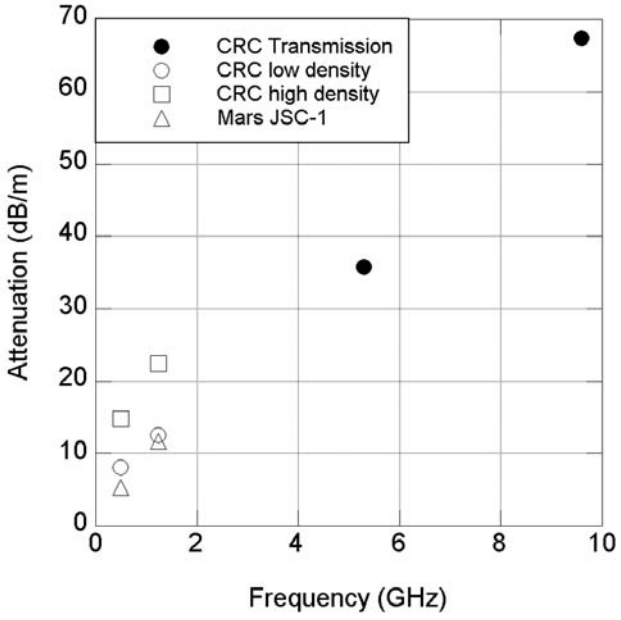

Figure 7. Attenuation over the portion of the electromagnetic spectrum considered in this study. Solid circles are transmission experiment results, open circles are predicted values from equation (1) using permittivity values of low-density CRC, open squares are predicted values for high-density CRC, and open triangles are predicted values for Mars JSC-1.

[25] As noted by *Schaber et al.* [1985, 1986], skin depth values can be misleading in discussions of penetration because radar signals have a two-way travel path through penetrated material. They therefore proposed using "radar imaging depth" (RID = skin depth/2) as a measure of the thickness of material through which an incident radar signal would decrease in strength by 1/e. This value is also discussed in the literature as "penetration depth" [e.g., *Campbell*, 2002]. Although not listed here, penetration depths can be derived by halving the values in Table 4. This gives values of 0.07 m at X band to 0.3–0.55 m at P band for CRC and 0.37 to 0.84 m from L to P band for Mars JSC-1.

[26] Although results of this study can be used to discuss the ability of radar to penetrate loose Martian sediments, it is noted that other factors also affect penetration. In fact, surface and volume scattering by surface and internal reflectors, respectively, can control whether a radar signal is able to reveal a buried surface. On the basis of orbital images (Figure 2), there may be areas on Mars covered by a homogeneous, rock-free dust (or sand) layer. In those areas, results of this study can be used to get a first order constraint on the thickness of Martian materials (similar to CRC and Mars JSC-1) that could be penetrated by radar at imaging radar frequencies.

[27] In an effort to constrain the expected thickness of dust in the low-inertia regions on Mars, *Christensen* [1986] used thermal, radar, and visual data to study regional dust deposits. He estimated that Martian dust ranges from 0.1 to $\sim$2 m in thickness. On the basis of calculations of radar penetration depths in this study, a P band SAR could reveal surfaces buried by up to $\sim$0.5 m of dust if Martian dust is compositionally similar to CRC. L band could image

through 0.2–0.35 m of dust, and even C band could image through slightly more than 0.1 m of dust. If these estimates are appropriate for Mars, radar operating at C band or lower frequency could penetrate the thinnest covers of dust determined by *Christensen* [1986], but even P band would not be able to penetrate the thickest deposits of 2 m to reveal obscured geology.

6. Conclusions

[28] The measurements of dielectric properties of Carbondale Red Clay and Mars JSC-1 soil simulant presented here are the first such measurements of these materials, and they complement other laboratory dielectric measurements [e.g., *Leuschen*, 1999; *Heggy et al.*, 2001; *Pettinelli et al.*, 2001] that also addressed the ability of radar to penetrate Martian surface materials. As illustrated by comparison of losses associated with CRC and Mars JSC-1 to losses from sand, it is important to consider various analogs that cover a range of possible compositional and physical characteristics of Martian materials.

[29] The relatively high losses observed in this study for metal-bearing, fine-grained materials suggest that radar operating at a frequency between P band and C band could penetrate thin (0.1 m) dust deposits on Mars. However, the radar penetration depth at P band for CRC is 0.3–0.55 m, less than the estimated maximum thickness of 2 m for dust on Mars [*Christensen*, 1986]. Therefore even the longest wavelength imaging radar would not penetrate the thickest estimated deposits of dust. In addition to the assumption that CRC is a good analog for Martian dust, these predictions also use the condition that a decrease in signal strength to less than ~37% of the incident signal would not be detected. If an instrument could detect lower signals, then the radar penetration depths would be greater than those discussed here. The dielectric values from this study could be used to predict penetration depths for any limit of signal detection.

[30] Until in situ dielectric measurements can be made on Mars or samples are returned to Earth, continued measurements of analog materials will be needed. When possible, measurements at temperatures and pressures approaching Martian conditions will result in more appropriate estimates of signal loss. Also because Martian materials can have a magnetic component, measurements of magnetic permeability should be included in future studies when appropriate [e.g., *Olhoeft*, 1998]. A more complete characterization of the loss factors of analogs for Martian surface materials will lead to more accurate predictions of radar performance at Mars.

[31] **Acknowledgments.** The authors thank C. Birtcher and G. Beardmore at ASU for help with the experiment, C. Santamarina for conducting the permittivity measurements, and T. Graff for providing the Mars JSC-1 material. We also thank J. van Zyl and B. Campbell for helpful discussions. Comments from J. Plaut and an anonymous reviewer greatly improved the manuscript. This work was supported by a NASA Graduate Student Researchers Program fellowship through JPL, a NASA/ASU Space Grant Consortium fellowship, and the Dr. Robert H. Goddard Scholarship from the National Space Club.

References

Allen, C. C., K. M. Jager, R. V. Morris, D. J. Lindstrom, M. M. Lindstrom, and J. P. Lockwood (1998), Martian soil simulant available for scientific, educational study, *Eos Trans. AGU*, *79*, 405–409.

Banin, A., B. C. Clark, and H. Wänke (1992), Surface chemistry and mineralogy, in *Mars*, edited by H. H. Kieffer et al., pp. 594–625, Univ. of Ariz. Press, Tucson.

Bell, J. F., et al. (1998), Mineralogy, composition, and origin of soil and dust at the Mars Pathfinder landing site, *Lunar Planet. Sci.*, [CD-ROM], *XXIX*, abstract 1723.

Bell, J. F., et al. (2004), Pancam multispectral imaging results from the Spirit rover at Gusev Crater, *Science*, *305*, 800–806.

Berlin, G. L., M. A. Tarabzouni, A. H. Al-Naser, K. M. Sheikho, and R. W. Larson (1986), SIR-B subsurface imaging of a sand-buried landscape: Al Labbah Plateau, Saudi Arabia, *IEEE Trans. Geosci. Remote Sens.*, *GE-24*, 595–602.

Birtcher, C. R. (1992), The electromagnetic anechoic chamber at Arizona State University: Characterization and measurements, M.S. thesis, 120 pp., Ariz. State Univ., Tempe.

Blom, R. G., R. E. Crippen, and C. Elachi (1984), Detection of subsurface features in SEASAT radar images of Means Valley, Mojave Desert, California, *Geology*, *12*, 346–349.

Campbell, B. A. (2002), *Radar Remote Sensing of Planetary Surfaces*, 331 pp., Cambridge Univ. Press, New York.

Campbell, B. A., R. E. Arvidson, M. K. Shepard, and R. A. Brackett (1997), Remote sensing of surface processes, in *Venus II: Geology, Geophysics, Atmosphere, and Solar Wind Environment*, edited by S. W. Bougher, D. M. Hunten, and R. J. Phillips, pp. 503–526, Univ. of Ariz. Press, Tucson.

Campbell, B. A., D. B. Campbell, J. A. Grant, S. Hensley, T. A. Maxwell, J. J. Plaut, P. Rosen, M. K. Shepard, and R. Simpson (2001), Orbital imaging radar and the search for water on Mars, paper presented at Conference on Geophysical Detection of Subsurface Water on Mars, Lunar and Planet. Inst., Houston, Tex.

Christensen, P. R. (1986), Regional dust deposits on Mars: Physical properties, age, and history, *J. Geophys. Res.*, *91*, 3533–3545.

Christensen, P. R. and H. J. Moore (1992), The Martian surface layer, in *Mars*, edited by H. H. Kieffer et al., pp. 686–729, Univ. of Ariz. Press, Tucson.

Christensen, P. R., et al. (2001), Mars Global Surveyor Thermal Emission Spectrometer experiment: Investigation description and surface science results, *J. Geophys. Res.*, *106*, 23,823–23,871.

Christensen, P. R., et al. (2003), Morphology and composition of the surface of Mars: Mars Odyssey THEMIS results, *Science*, *300*, 2056–2061.

Clark, B. C., A. K. Baird, R. J. Weldon, D. M. Tsusaki, L. Schnabel, and M. P. Candelaria (1982), Chemical composition of Martian fines, *J. Geophys. Res.*, *87*, 10,059–10,067.

Cutts, J. A., and R. S. U. Smith (1973), Aeolian deposits and dunes on Mars, *J. Geophys. Res.*, *78*, 4139–4154.

Dabbagh, A. E., K. G. Al-Hinai, and M. A. Khan (1997), Detection of sand-covered geologic features using SIR-C/X-SAR data, *Remote Sens. Environ.*, *59*, 375–382.

Davis, P. A., C. S. Breed, J. F. McCauley, and G. G. Schaber (1993), Surficial geology of the Safsaf region, south-central Egypt, derived from remote-sensing and field data, *Remote Sens. Environ.*, *46*, 183–203.

Downs, G. S., R. M. Goldstein, R. R. Green, G. A. Morris, and P. E. Reichley (1973), Martian topography and surface properties as seen by radar: The 1971 opposition, *Icarus*, *18*, 8–21.

Elachi, C., L. E. Roth, and G. Schaber (1984), Spaceborne radar subsurface imaging in hyperarid regions, *IEEE Trans. Geosci. Remote Sens.*, *GE-22*, 383–387.

Farr, T. G., C. Elachi, P. Hartl, and K. Chowdhury (1986), Microwave penetration and attenuation in desert soil: A field experiment with the Shuttle Imaging Radar, *IEEE Trans. Geosci. Remote Sens.*, *GE-24*, 590–594.

Gellert, R., et al. (2004), Chemistry of rocks and soils in Gusev Crater from the Alpha Particle X-ray Spectrometer, *Science*, *305*, 829–832.

Grant, J. A., A. E. Schutz, and B. A. Campbell (2003), Ground-penetrating radar as a tool for probing the shallow subsurface of Mars, *J. Geophys. Res.*, *108*(E4), 8024, doi:10.1029/2002JE001856.

Greeley, R., N. Lancaster, S. Lee, and P. Thomas (1992), Martian aeolian processes, sediments, and features, in *Mars*, edited by H. H. Kieffer et al., pp. 730–766, Univ. of Ariz. Press, Tucson.

Greeley, R., K. Bender, P. E. Thomas, G. Schubert, D. Limonadi, and C. M. Weitz (1995), Wind-related features and processes on Venus: Summary of Magellan results, *Icarus*, *115*, 399–420.

Guo, H., G. G. Schaber, C. S. Breed, and A. J. Lewis (1986), Shuttle Imaging Radar response from sand and subsurface rocks of Alashan Plateau in north-central China, in *International Symposium on Remote Sensing for Resources Development and Environmental Management 7th Proceedings, ISPRS Commission VII, Enschede, Netherlands, August 25–29, 1986*, pp. 137–143, A. A. Balkema, Brookfield, Vt.

Heggy, E., P. Paillou, G. Ruffie, J. M. Malezieux, F. Costard, and G. Grandjean (2001), On water detection in the Martian subsurface using sounding radar, *Icarus*, *154*, 244–257.

Heggy, E., P. Paillou, F. Costard, N. Mangold, G. Ruffie, F. Demontoux, G. Grandjean, and J. M. Malézieux (2003), Local geoelectrical models of the Martian subsurface for shallow groundwater detection using sounding radars, *J. Geophys. Res.*, *108*(E4), 8030, doi:10.1029/2002JE001871.

Hoekstra, P., and A. Delaney (1974), Dielectric properties of soils at UHF and microwave frequencies, *J. Geophys. Res.*, *79*, 1699–1708.

Hunt, G. R., L. M. Logan, and J. W. Salisbury (1973), Mars: Component of infrared spectra and composition of the dust cloud, *Icarus*, *18*, 459–469.

Hviid, S. F., et al. (1997), Magnetic properties experiments on the Mars Pathfinder Lander: Preliminary results, *Science*, *278*, 1768–1770.

Hviid, S. F., et al. (2004), Preliminary results of the magnetic properties experiments on the Mars Exploration Rovers, Spirit and Opportunity, *Proc. Lunar Planet. Sci. Conf. 35th*, abstract 2177.

Lancaster, N., G. G. Schaber, and J. T. Teller (2000), Orbital radar studies of paleodrainages in the central Namib Desert, *Remote Sens. Environ.*, *71*, 216–225.

Leuschen, C. J. (1999), Analysis of the complex permittivity and permeability of a Martian soil simulant from 1 MHz to 1 GHz, paper presented at IEEE International Symposium on Geoscience and Remote Sensing, Inst. of Electr. and Electron. Eng., Hamburg, Germany.

Leuschen, C., S. Clifford, and P. Gogineni (2003a), Simulation of a surface-penetrating radar for Mars exploration, *J. Geophys. Res.*, *108*(E4), 8035, doi:10.1029/2002JE001875.

Leuschen, C., P. Kanagaratnam, K. Yoshikawa, S. Arcone, and P. Gogineni (2003b), Design and field experiments of a ground-penetrating radar for Mars exploration, *J. Geophys. Res.*, *108*(E4), 8034, doi:10.1029/2002JE001876.

Malin, M. C., and K. S. Edgett (2001), Mars Global Surveyor Mars Orbiter Camera: Interplanetary cruise through primary mission, *J. Geophys. Res.*, *106*, 23,429–23,570.

Mätzler, C. (1998), Microwave permittivity of dry sand, *IEEE Trans. Geosci. Remote Sens.*, *36*, 317–319.

McCauley, J. F., M. H. Carr, J. A. Cutts, W. K. Hartmann, H. Masursky, D. J. Milton, R. P. Sharp, and D. E. Wilhelms (1972), Preliminary Mariner 9 report on the geology of Mars, *Icarus*, *17*, 289–327.

McCauley, J. F., G. G. Schaber, C. S. Breed, M. J. Grolier, C. V. Haynes, B. Issawi, C. Elachi, and R. Blom (1982), Subsurface valleys and geoarchaeology of the eastern Sahara revealed by shuttle radar, *Science*, *218*, 1004–1020.

Morris, R. V., et al. (2004), Mineralogy at Gusev Crater from the Mössbauer Spectrometer on the Spirit Rover, *Science*, *305*, 833–836.

Olhoeft, G. R. (1989), Electrical properties of rocks, in *Physical Properties of Rocks and Minerals*, edited by Y. S. Touloukian, W. R. Judd, and R. F. Roy, pp. 257–330, Taylor and Francis, Philadelphia, Pa.

Olhoeft, G. R. (1998), Ground penetrating radar on Mars, paper presented at GPR '98, Seventh International Conference on Ground Penetrating Radar, Univ. of Kansas, Lawrence.

Olhoeft, G. R. and D. E. Capron (1993), Laboratory measurements of the radiofrequency electrical and magnetic properties of soils from near Yuma, Arizona, *U.S. Geol. Surv. Open File Rep.*, *93–701*.

Olhoeft, G. R. and D. E. Capron (1994), Petrophysical causes of electromagnetic dispersion, paper presented at GPR 1994: Fifth International Conference on Ground Penetrating Radar, Kitchener, Ontario, Canada.

Olhoeft, G. R., and D. W. Strangway (1974), Electrical properties of the surface layers of Mars, *Geophys. Res. Lett.*, *1*(3), 141–143.

Olhoeft, G. R., and D. W. Strangway (1975), Dielectric properties of the first 100 meters of the Moon, *Earth Planet. Sci. Lett.*, *24*, 394–404.

Paillou, P., T. W. Thompson, J. J. Plaut, P. A. Rosen, S. Hensley, C. Elachi, D. Massonnet, and J. Achache (2001), MEEM: An orbital synthetic aperture radar for Mars exploration, paper presented at Conference on Geophysical Detection of Subsurface Water on Mars, Lunar and Planet. Inst., Houston, Tex.

Pettinelli, E., G. Della Monica, F. Bella, G. Losito, R. Di Maio, G. Vannaroni, M. Storini, S. Orsini, and R. Cerulli-Irelli (2001), High and low frequency electrical measurements of Martian soil simulants, paper presented at Conference on Geophysical Detection of Subsurface Water on Mars, Lunar and Planet. Inst., Houston, Tex.

Rieder, R., T. Economou, H. Wanke, A. Turkevich, J. Crisp, J. Bruckner, G. Dreibus, and H. Y. McSween Jr. (1997), The chemical composition if Martian soil and rocks returned by the Mobile Alpha Proton X-ray Spectrometer: Preliminary results from the x-ray mode, *Science*, *278*, 1771–1774.

Safaeinili, A., et al. (2001), Radar sounding of Mars: A focus on MARSIS, paper presented at Conference on Geophysical Detection of Subsurface Water on Mars, Lunar and Planet. Inst., Houston, Tex.

Schaber, G. G., and C. S. Breed (1999), The importance of SAR wavelength in penetrating blow sand in northern Arizona, *Remote Sens. Environ.*, *69*, 87–104.

Schaber, G. G., C. S. Breed, J. F. McCauley, and G. H. Billingsley (1985), Physical controls on SIR-A signal penetration and subsurface scattering in the Mars-like Eastern Sahara (abstract), *Proc. Lunar Planet. Sci. Conf. 16th*, 732–733.

Schaber, G. G., J. F. McCauley, C. S. Breed, and G. R. Olhoeft (1986), Shuttle imaging radar: Physical controls on signal penetration and scattering in the eastern Sahara, *IEEE Trans. Geosci. Remote Sens.*, *GE-24*, 603–623.

Schaber, G. G., J. F. McCauley, and C. S. Breed (1997), The use of multifrequency and polarimetric SIR-C/X-SAR data in geologic studies of Bir Safsaf, Egypt, *Remote Sens. Environ.*, *GE-59*, 337–363.

Seu, R., R. Orosei, D. Biccari, and A. Masdea (2003), The MRO Subsurface Sounding Shallow Radar (SHARAD), in *Sixth International Conference on Mars* [CD-ROM], abstract 3079, Lunar and Planet. Inst., Houston, Tex.

Thompson, T. W., J. J. Plaut, R. E. Arvidson, and P. Paillou (2000), Orbital synthetic aperture radar (SAR) for Mars post sample return exploration, *Lunar Planet. Sci.*, *XXXI*, abstract 1161.

Toulmin, P., A. K. Baird, B. C. Clark, K. Kiel, H. J. Rose Jr., R. P. Christian, P. H. Evans, and W. C. Kelliher (1977), Geochemical and mineralogical interpretation of the Viking inorganic chemical results, *J. Geophys. Res.*, *82*, 4625–4634.

Ulaby, F. T., M. K. Moore, and A. K. Fung (1986), *Microwave Remote Sensing, Active and Passive*, vol. 3, Artech House, Norwood, Mass.

Von Hippel, A. R. (1954), *Dielectrics and Waves*, pp. 26–37, J. Wiley, Hoboken, N. J.

Wang, J. R., and T. J. Schmugge (1980), An empirical model for the complex dielectric permittivity of soils as a function of water content, *IEEE Trans. Geosci. Remote Sens.*, *GE-18*, 288–295.

White, B. R., B. M. Lacchia, R. Greeley, and R. N. Leach (1997), Aeolian behavior of dust in a simulated Martian environment, *J. Geophys. Res.*, *102*, 25,629–25,640.

Williams, K. K., and R. Greeley (2001), Radar attenuation by sand: Laboratory measurements of radar transmission, *IEEE Trans. Geosci. Remote Sens.*, *39*, 2521–2526.

Williams, K. K., and R. Greeley (2004), Laboratory and field measurements of the modification of radar backscatter by sand, *Remote Sens. Environ.*, *89*, 29–40.

R. Greeley, Department of Geological Sciences, Arizona State University, Box 871404, Tempe, AZ 85287-1404, USA.

K. K. Williams, Center for Earth and Planetary Studies, National Air and Space Museum, MRC 315, P.O. Box 37012, Washington, DC 20013-7012, USA. (williamsk@nasm.si.edu)